energies

MDPI

Article

A Simplified Space Vector Pulse Width Modulation Algorithm of a High-Speed Permanent Magnet Synchronous Machine Drive for a Flywheel Energy Storage System

Hongjin Hu †, Haoze Wang †, Kun Liu *, Jingbo Wei and Xiangjie Shen

School of Aeronautics and Astronautics, Sun Yat-Sen University, Shenzhen 518107, China; huhj25@mail2.sysu.edu.cn (H.H.); wanghz5@mail.sysu.edu.cn (H.W.); weijb5@mail.sysu.edu.cn (J.W.); shenxj7@mail2.sysu.edu.cn (X.S.)

* Correspondence: liukun6@mail.sysu.edu.cn

† These authors contributed equally to this work.

Abstract: A space vector pulse width modulation (SVPWM) algorithm is an important part of the permanent magnet synchronous machine (PMSM) drive to achieve direct current (DC) to alternating current (AC) conversion. The execution of the conventional SVPWM algorithm is a complex process which will limit the sampling frequency of the high-speed PMSM drive. Low sampling frequency will cause high current total harmonic distortion (THD) and eddy current loss. To increase the sampling frequency, this paper proposes a novel simplified SVPWM algorithm. The proposed SVPWM algorithm turns the vector composition problem of the conventional SVPWM algorithm into an optimization problem of the dwell time of the basic vector. The proposed SVPWM algorithm has an optimal vector dwell time (OVDT). The dwell time of the basic vector can be directly calculated by solving the optimization problem. The proposed SVPWM algorithm does not need sector identification compared to the conventional algorithm. The experiments of the proposed SVPWM algorithm are performed in a high-speed PMSM drive of a flywheel energy storage system (FESS). Compared to the conventional SVPWM algorithm, the execution time of the proposed SVPWM algorithm is reduced by 38%. By using the proposed SVPWM algorithm, the sampling frequency can be increased from 33 kHz to 40 kHz. With the higher sampling frequency, the current THD is reduced by 25.6%. The effectiveness of the proposed simplified SVPWM algorithm is verified experimentally.

Keywords: SVPWM; high-speed PMSM; FESS; PMSM drive; optimal vector dwell time

Citation: Hu, H.; Wang, H.; Liu, K.; Wei, J.; Shen, X A Simplified Space Vector Pulse Width Modulation Algorithm of a High-Speed Permanent Magnet Synchronous Machine Drive for a Flywheel Energy Storage System. *Energies* **2022**, *15*, 4065. https://doi.org/10.3390/en15114065

Academic Editor: Armando Pires

Received: 4 May 2022
Accepted: 30 May 2022
Published: 1 June 2022

1. Introduction

Energy storage systems (ESSs) play an increasingly significant role in industrial applications. Among the variety of ESSs, the flywheel energy storage system (FESS) has several advantages, including fast response, high instantaneous power, high energy efficiency, little maintenance tasks, and long lifetime [1–4]. As a result, FESS has been utilized in many applications, such as electric vehicles [5,6], railways [7], wind generators [8], photovoltaic systems [9], distribution networks [10], and UPS systems [11,12]. FESS is a type of mechanical energy storage device in which the mechanical energy is stored in a high-rotation-speed flywheel rotor. The mutual conversion of mechanical energy and electric energy uses a high-speed machine. Among the variety of machine types, the permanent magnet synchronous machine (PMSM) is the most commonly used type in FESS [1,13]. To achieve PMSM control, a field-oriented control (FOC) generally applies. When the PMSM operates at a high speed, the frequency of the current is high. The control system with a low sampling frequency cannot offer a high control accuracy and cause a large time delay, which will cause a high current total harmonic distortion (THD) and degenerate the performance of the FESS [14,15]. In general, a PMSM FOC mainly includes space vector pulse width modulation (SVPWM), coordinate transformation, and the calculation of the

control law [16]. SVPWM is one of the time consumption processes for the FOC. The time consumption of the SVPWM can be reduced by simplifying the SVPWM algorithm. Therefore, simplifying the SVPWM algorithm is an efficient way for the PMSM control system to achieve a high sampling frequency.

To simplify the SVPWM algorithm, many methods have been proposed in the past decades. The conventional SVPWM algorithm is based on an orthogonal α–β coordinate system. In the α–β coordinate system, the sector can be identified and the dwell time can be calculated by the relationship among the reference vectors, V_α and V_β, and DC-link voltage. In [17], the effective time concept is utilized to avoid sector identification, which can simplify the modulation task. To simplify sector identification, an improved sector identification method that adds sign detection is proposed in [18]. In [19], a simplified SVPWM algorithm is proposed for the multiphase machine drive, which has the two modulation steps of offline virtual voltage vectors construction and real-time implementation. In [20], a simplified SVPWM technique is proposed for the four-switch three-phase grid-side converter. Based on the programmable gate array (FPGA) feature, an efficient SVPWM algorithm is proposed in [21]. In [22], virtual vectors are adopted to simplify the SVPWM and reduce the error of reference voltage composition. In the orthogonal α–β coordinate system, the relationship of the vector composition can be intuitively derived. However, the α–β coordinate system is not beneficial for fast sector identification and dwell time calculation. To simplify the SVPWM algorithm, several methods based on nonorthogonal coordinates have been proposed. SVPWM algorithms based on the a-b-c coordinate systems [23,24], 60° coordinate systems [25], and barycentric coordinates [26] are proposed. For the above SVPWM algorithm, the sector is identified and the dwell time is calculated in real time. Sector identification and dwell time calculation can also be executed offline. Creating an offline look-up table of the relationship among the sector identification, vector dwell time, and reference vector is an efficient way to simplify the SVPWM algorithm. In [27], a novel look-up table, called human eyes, is established to identify the sector. In [28–30], the relationship among the sector identification, vector dwell time, and reference vector is established by artificial neural networks (ANNs) to simplify the SVPWM algorithm. The time consumption of the SVPWM algorithm can be significantly reduced by identifying the sector and calculating dwell time offline. However, these algorithms cause high memory overhead for the micro controller unit (MCU). Using an approximate function to establish the relationship between the duty cycle and reference vector is also an efficient way to simplify the modulation task. The third harmonic injection method is generally used to establish the relationship between the duty cycle and reference vector [31,32]. However, the approximate function method would have a degenerative effect on harmonic performance.

The purpose of the SVPWM algorithm is to compose the reference vector by using the basic vectors. In the above algorithms, the dwell time of each basic vector is deduced from the perspective of the vector composition of geometry. The derivation of these SVPWM algorithms has an intuitive geometric concept, and these SVPWM algorithms have been practically applied. However, the derivation from the perspective of geometry needs to divide the space into several sectors or regions, which is one of the factors that increase the complexity of the SVPWM algorithm.

In this paper, a new simplified SVPWM algorithm is proposed from the perspective of optimization. According to linear space theory, the vector composition problem of the conventional SVPWM algorithm can be transformed into a linear equation problem. A linear equation is an overdetermined equation because there are enough basic vectors to compose the reference vector. An overdetermined equation has infinite solutions which need to find the optimal solution. Thus, the vector composition problem of the SVPWM algorithm can be transformed into an optimization problem. By solving the optimization problem, sector identification in the conventional SVPWM algorithm can be avoided, which makes the SVPWM algorithm simpler. The SVPWM algorithm deduced from the perspective of optimization has an optimal vector dwell time (OVDT), and the OVDTs of

the 1-norm and 2-norm are adopted in this paper. The novelty and contribution of this paper consist of:

(1) We propose a new SVPWM algorithm based on the perspective of optimization to derive the dwell time. The theoretical derivation and the flowcharts of the proposed SVPWM algorithm are presented. Compared with the conventional algorithm, the proposed SVPWM algorithm needs less equation expression and logical judgment to perform the modulation task.
(2) The implementation of the proposed SVPWM algorithm in a high-speed PMSM drive of FESS is reported.
(3) We report a comparison of the execution times of the proposed SVPWM algorithm, conventional SVPWM algorithm, and SVPWM algorithms in [17,18,31].

The remainder of this paper is organized as follows. In Section 2, the basic principle of SVPWM is described. In Section 3, the SVPWM algorithm with OVDT is proposed, the optimization problem is presented, and the optimal solutions of the 1-norm and 2-norm are deduced. In Section 4, experiments are performed on a 8 kW/36,000 rpm FESS prototype to verify the proposed SVPWM algorithm. The conclusions are drawn in Section 5. Finally, future work is presented in Section 6.

2. Description of SVPWM of PMSM Drive

The general topology of the PMSM drive of the FESS is shown in Figure 1. To obtain a three-phase sinusoidal current, the PMSM drive should generate a reference vector $\mathbf{V_r}$ in a circular motion. The PMSM drive can generate eight vectors $\mathbf{V_0}$, $\mathbf{V_1}$, ..., $\mathbf{V_7}$, as shown in Figure 2a. $\mathbf{V_1}$, $\mathbf{V_2}$, ..., and $\mathbf{V_6}$ are nonzero vectors, and $\mathbf{V_0}$ and $\mathbf{V_7}$ are zero vectors. Space can be divided into six sectors by the six nonzero vectors. For the conventional SVPWM algorithm, $\mathbf{V_r}$ is composed of adjacent nonzero vectors. When the reference vector is located in sector I, the adjacent vectors are $\mathbf{V_4}$ and $\mathbf{V_6}$, as shown in Figure 2b. The reference vector is composed of $\mathbf{V_4}$ and $\mathbf{V_6}$, presented as (1).

$$\mathbf{V_r} = \frac{t_4}{T_s}\mathbf{V_4} + \frac{t_6}{T_s}\mathbf{V_6} \tag{1}$$

where T_s is the period of the PWM signal and t_4 and t_6 are the dwell times of $\mathbf{V_4}$ and $\mathbf{V_6}$, respectively.

The dwell time is generally deduced in an orthogonal α–β coordinate system, which is presented as

$$\begin{cases} t_4 = \frac{T_s\left(\sqrt{3}|\mathbf{V}_\alpha| - |\mathbf{V}_\beta|\right)}{\sqrt{3}|\mathbf{V_4}|} \\ t_6 = \frac{2\sqrt{3}T_s}{3}\frac{|\mathbf{V}_\beta|}{|\mathbf{V_6}|} \\ t_0 = t_7 = \frac{T_s - t_6 - t_4}{2} \end{cases} \tag{2}$$

where t_7 and t_0 are the dwell times of $\mathbf{V_0}$ and $\mathbf{V_7}$, and $\mathbf{V}_\alpha$ and $\mathbf{V}_\beta$ are the projections of $\mathbf{V_r}$ on the α and β axes.

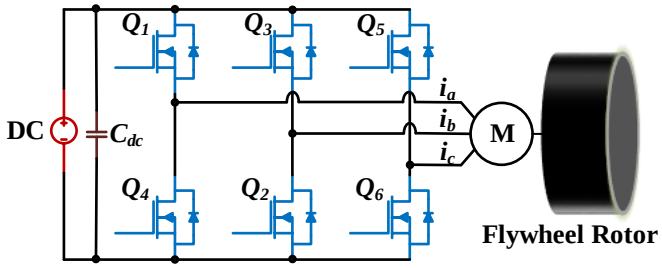

Figure 1. The topology of the PMSM drive of FESS.

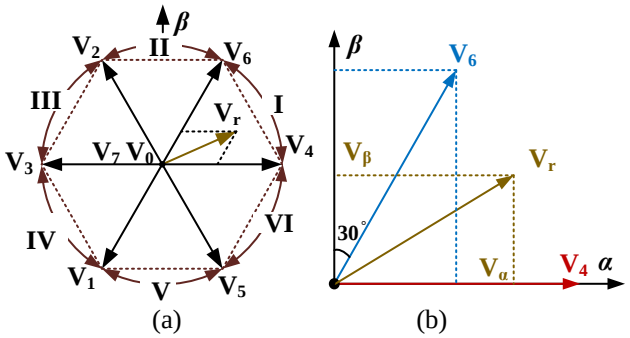

Figure 2. (**a**) The space vector of the PMSM drive. (**b**) The vector composition in sector I.

From (2), the duty cycles of the PWM signals can be deduced as

$$\begin{cases} d_a = \frac{t_4+t_6+t_7}{T_s} \\ d_b = \frac{t_6+t_7}{T_s} \\ d_c = \frac{t_7}{T_s} \end{cases}. \tag{3}$$

The center-aligned PWM signal in sector I and the duty cycle in one period are shown in Figure 3. The conventional SVPWM algorithm needs to identify the sector, calculate the dwell time of the vectors, and finally obtain the duty cycles. The conventional SVPWM algorithm has a high time consumption for the high-speed PMSM drive, which needs a high sampling frequency.

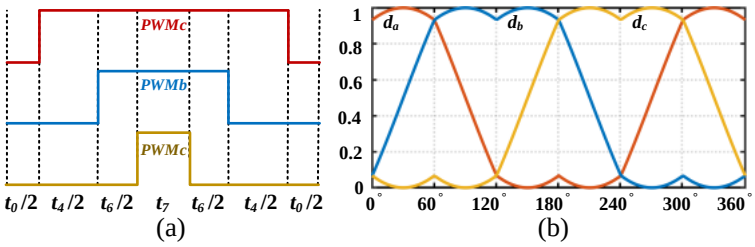

Figure 3. (**a**) The PWM signal in sector I. (**b**) The duty cycle in one period.

3. Proposed SVPWM Algorithm with OVDT

The conventional SVPWM algorithm is derived from the vector composition of the geometry. To simplify the SVPWM algorithm, this paper turns the geometrical vector composition problem into an optimization problem.

3.1. Optimization Problem in SVPWM

To turn the vector composition problem into an optimization problem, the six nonzero vectors are redefined as in (4).

$$\begin{cases} \mathbf{V_a} = \mathbf{V_4}, & -\mathbf{V_a} = \mathbf{V_3} \\ \mathbf{V_b} = \mathbf{V_2}, & -\mathbf{V_b} = \mathbf{V_5} \\ \mathbf{V_c} = \mathbf{V_1}, & -\mathbf{V_c} = \mathbf{V_6} \end{cases} \tag{4}$$

The redefined nonzero vectors are shown in Figure 4a. The purpose of the SVPWM algorithm is to compose the reference vector through the six nonzero vectors. Figure 4b shows the projection of the reference vectors onto the α–β coordinates. From Figure 4b, the relationship among $\mathbf{V_a}$, $\mathbf{V_b}$, $\mathbf{V_c}$, and $\mathbf{V_r}$ can be deduced as in (5).

$$\begin{cases} \frac{t_a}{T_s}|\mathbf{V_a}| - \frac{t_b}{2T_s}|\mathbf{V_b}| - \frac{t_c}{2T_s}|\mathbf{V_c}| = V_{r\alpha} \\ \frac{\sqrt{3}t_b}{2T_s}|\mathbf{V_b}| - \frac{\sqrt{3}t_c}{2T_s}|\mathbf{V_c}| = V_{r\beta} \end{cases} \tag{5}$$

where t_a, t_b, and t_c are the dwell times of $\mathbf{V_a}$, $\mathbf{V_b}$, and $\mathbf{V_c}$, respectively, and $V_{r\alpha}$ and $V_{r\beta}$ are the projections of $\mathbf{V_r}$ onto the α–β coordinates.

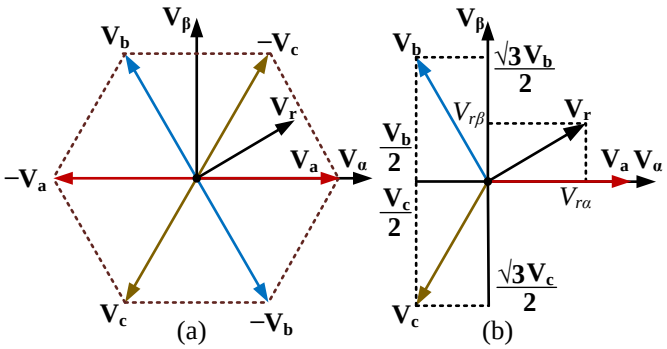

Figure 4. (**a**) The redefined space vectors. (**b**) The vector projection onto the α–β coordinate.

When t_a, t_b, or t_c is smaller than zero, the vector $-\mathbf{V_a}$, $-\mathbf{V_b}$, or $-\mathbf{V_c}$ is applied. Linear Equation (5) can be reformatted in matrix form, presented as (6).

$$\begin{bmatrix} 1 & -\frac{1}{2} & -\frac{1}{2} \\ 0 & \frac{\sqrt{3}}{2} & -\frac{\sqrt{3}}{2} \end{bmatrix} \begin{bmatrix} t_a \\ t_b \\ t_c \end{bmatrix} = \begin{bmatrix} V_\alpha \\ V_\beta \end{bmatrix} \tag{6}$$

where

$$V_a = \frac{T_s V_{ra}}{|\mathbf{V_a}|} \text{ and } V_\beta = \frac{T_s V_{r\beta}}{|\mathbf{V_a}|}.$$

Because Linear Equation (6) is an overdetermined equation, it has infinite solutions. This means that the reference vector can be composed of infinite combinations of the vectors. For the conventional SVPWM algorithm, a combination of adjacent vectors is selected to compose the reference vector. In this paper, the proposed SVPWM algorithm finds a combination of vectors that possesses an optimal dwell time. The optimization problem in SVPWM can be described as

$$\begin{aligned} &\min f(t_a, t_b, t_c) \\ &s.t. \begin{bmatrix} 1 & -\frac{1}{2} & -\frac{1}{2} \\ 0 & \frac{\sqrt{3}}{2} & -\frac{\sqrt{3}}{2} \end{bmatrix} \begin{bmatrix} t_a \\ t_b \\ t_c \end{bmatrix} = \begin{bmatrix} V_\alpha \\ V_\beta \end{bmatrix} \end{aligned} \tag{7}$$

where $f(t_a, t_b, t_c)$ is the cost function.

3.2. Optimal Solution of the 1-Norm

When the cost function is 1-norm, the optimization problem is described as

$$\begin{aligned} &\min f_1 = \|\mathbf{T}\|_1 = |t_a| + |t_b| + |t_c| \\ &s.t. \begin{bmatrix} 1 & -\frac{1}{2} & -\frac{1}{2} \\ 0 & \frac{\sqrt{3}}{2} & -\frac{\sqrt{3}}{2} \end{bmatrix} \begin{bmatrix} t_a \\ t_b \\ t_c \end{bmatrix} = \begin{bmatrix} V_\alpha \\ V_\beta \end{bmatrix}. \end{aligned} \tag{8}$$

where $\mathbf{T} = [t_a, t_b, t_c]^T$.

To solve the optimization problem, the constrained optimization problem of (8) needs to be transformed into an unconstrained optimization problem. Substituting the constraint condition into the cost function, the unconstrained optimization problem is presented as

$$\min f_1 = |t_c + a| + |t_c + b| + |t_c| \tag{9}$$

where

$$a = V_\alpha + \frac{\sqrt{3}}{3}V_\beta \; and \; b = \frac{2\sqrt{3}}{3}V_\beta.$$

The minimum value of f_1 should satisfy the condition of (10).

$$f_1{}'(\tau_{c1} + |\varepsilon|) > 0, \quad f_1{}'(\tau_{c1} - |\varepsilon|) \; < 0 \tag{10}$$

where τ_{c1} is the optimal dwell time of $\mathbf{V_c}$, ε is dimensionless, and $f_1{}'$ is the first derivative of f_1.

The first derivative of f_1 can be deduced as

$$f_1{}' = \mathrm{sgn}(t_c) + \mathrm{sgn}(t_c + a) + \mathrm{sgn}(t_c + b). \tag{11}$$

where sgn is a sign function.

$f_1{}'(\tau_{c1}+|\varepsilon|)$ and $f_1{}'(\tau_{c1}\text{-}|\varepsilon|)$ can be deduced as in (12).

$$\begin{cases} f_1{}'(t_c + |\varepsilon|) = f_1{}'(t_c) + f_1{}''(t_c)|\varepsilon| \\ f_1{}'(t_c - |\varepsilon|) = f_1{}'(t_c) - f_1{}''(t_c)|\varepsilon| \end{cases} \tag{12}$$

where $f_1{}''$ is the second derivative of f_1.

$f_1{}''$ can be deduced as

$$f_1{}'' = \delta(t_c) + \delta(t_c + a) + \delta(t_c + b). \tag{13}$$

where δ is the Dirac delta function.

According to the definition of the Dirac delta function, when $t_c \neq 0$, $t_c \neq -a$, or $t_c \neq -b$, $f_1{}''$ is zero. Thus, $f_1{}'(\tau_{c1} + |\varepsilon|)$ is equal to $f_1{}'(\tau_{c1} - |\varepsilon|)$, which is presented as (14).

$$f_1{}'(t_c \; + \; |\varepsilon|) = f_1{}'(t_c \; - \; |\varepsilon|) \tag{14}$$

According to (10) and (14), the minimum value of f_1 will not occur in $t_c \neq 0$, $t_c \neq -a$, or $t_c \neq -b$. Therefore, the minimum value occurs only in $t_c = 0$, $t_c = -a$, or $t_c = -b$. Through a method of exhaustion, the optimal t_c of the 1-norm can be obtained, which is presented as

$$\tau_{c1} = \begin{cases} -a, & |a| \geq |b|, |a| > |c| \\ 0, & |c| \geq |a|, |c| > |b| \\ -b, & |b| \geq |c|, |b| > |a| \end{cases} \tag{15}$$

where $c = a - b$. The optimal τ_{a1} and τ_{b1} are presented in (16).

$$\begin{cases} \tau_{a1} = \tau_c + a \\ \tau_{b1} = \tau_c + b \end{cases} \tag{16}$$

According to (15) and (16), one of the dwell times among τ_{a1}, τ_{b1}, and τ_{c1} must be zero, and the plus-minus sign of the nonzero dwell time is the opposite. When $|b| \geq |c|$ and $|b| > |a|$, the dwell time of $\mathbf{V_b}$ is zero. The reference vector is composed of $\mathbf{V_a}$ and $-\mathbf{V_c}$ or $-\mathbf{V_a}$ and $\mathbf{V_c}$, and the corresponding center-aligned PWM signal is shown in Figure 5. When $\mathbf{V_r}$ is composed of the vectors $\mathbf{V_a}$ and $-\mathbf{V_c}$, the duty cycle is deduced as in (17).

$$\begin{cases} d_{a1} = \frac{\tau_a - \tau_c + t_7}{T_s} \\ d_{b1} = \frac{-\tau_c + t_7}{T_s} \\ d_{c1} = \frac{t_7}{T_s} \end{cases} \tag{17}$$

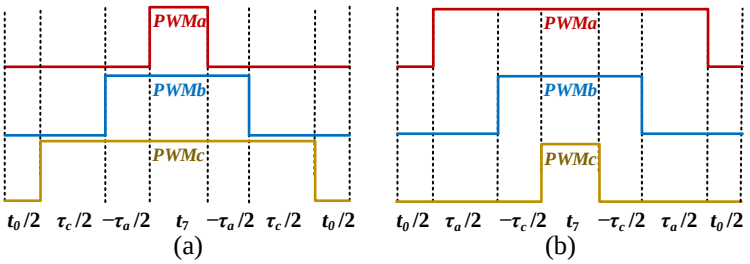

Figure 5. The PWM signals when $\tau_{b1} = 0$. (**a**) The PWM signal with the vectors $-\mathbf{V}_a$ and $\mathbf{V_c}$. (**b**) The PWM signal with the vectors $\mathbf{V_a}$ and $-\mathbf{V_c}$.

The dwell time of the zero vector t_7 can be deduced as

$$t_7 = \frac{T_s - (t_a - t_c)}{2} \tag{18}$$

Substituting (18) into (17), the duty cycle calculated expression can be further deduced as shown in (19).

$$\begin{cases} d_{a1} = \frac{T_s+\tau_a-\tau_c}{2T_s} = \frac{T_s+\tau_a-\tau_b-\tau_c}{2T_s} \\ d_{b1} = \frac{T_s+\tau_c-\tau_a}{2T_s} = \frac{T_s+\tau_b-\tau_a-\tau_c}{2T_s} \\ d_{c1} = \frac{T_s-\tau_a-\tau_c}{2T_s} = \frac{T_s+\tau_c-\tau_a-\tau_c}{2T_s} \end{cases} \tag{19}$$

When $\mathbf{V_r}$ is composed of the vectors $-\mathbf{V_a}$ and $\mathbf{V_c}$, the duty cycle can be deduced according to (20).

$$\begin{cases} d_{a1} = \frac{t_7}{T_s} \\ d_{b1} = \frac{-\tau_a+t_7}{T_s} \\ d_{c1} = \frac{\tau_c-\tau_a+t_7}{T_s} \end{cases} \tag{20}$$

Substituting (18) into (20), the same calculated expression of (19) is obtained. Similarly, when $|a| \geq |b|$, $|a| > |c|$ or $|c| \geq |a|$, and $|c| > |b|$, the duty cycle calculation expression is the same as that of (19). When (15) and (19) are combined, the duty cycle of the SVPWM with the optimal solution of the 1-norm can be summarized as shown in (21), (22), and (23) respectively.

$$\begin{cases} d_{a1} = \frac{c}{2T_s} + \frac{1}{2} \\ d_{b1} = \frac{-c}{2T_s} + \frac{1}{2} \\ d_{c1} = \frac{-a-b}{2T_s} + \frac{1}{2} \end{cases}, \quad |c| \geq |a|,\ |c| > |b| \tag{21}$$

$$\begin{cases} d_{a1} = \frac{a}{2T_s} + \frac{1}{2} \\ d_{b1} = \frac{b-c}{2T_s} + \frac{1}{2} \\ d_{c1} = \frac{-a}{2T_s} + \frac{1}{2} \end{cases}, \quad |a| \geq |b|,\ |a| > |c| \tag{22}$$

$$\begin{cases} d_{a1} = \frac{a+b}{2T_s} + \frac{1}{2} \\ d_{b1} = \frac{b}{2T_s} + \frac{1}{2} \\ d_{c1} = \frac{-b}{2T_s} + \frac{1}{2} \end{cases}, \quad |b| \geq |c|,\ |b| > |a| \tag{23}$$

From (21) to (23), the duty cycle of SVPWM can be directly calculated. The duty cycle of one period is shown in Figure 6. For the SVPWM algorithm with the OVDT of the 1-norm, the reference vector is composed of two nonzero vectors, which is the same as the conventional SVPWM algorithm. Thus, the duty cycle waveform is the same as the waveform of the conventional SVPWM algorithm. The conventional SVPWM algorithm has six equation expressions to calculate the duty cycles of six sectors [18]. From (21) to (23), the SVPWM algorithm with the OVDT of the 1-norm only needs three equation expressions

to calculate the duty cycle. In addition, the proposed SVPWM algorithm needs less logical judgment. Thus, the proposed SVPWM algorithm is simpler.

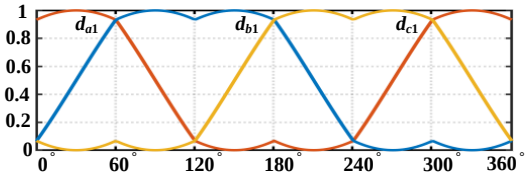

Figure 6. The duty cycle of SVPWM algorithm with the optimal dwell time of the 1-norm.

3.3. Optimal Solution of the 2-Norm

When the cost function is 2-norm, the optimization problem is as presented in (24).

$$\begin{aligned} &\min f_2 = \|\mathbf{T}\|_2 = {t_a}^2 + {t_b}^2 + {t_c}^2 \\ &s.t. \begin{bmatrix} 1 & -\frac{1}{2} & -\frac{1}{2} \\ 0 & \frac{\sqrt{3}}{2} & -\frac{\sqrt{3}}{2} \end{bmatrix} \begin{bmatrix} t_a \\ t_b \\ t_c \end{bmatrix} = \begin{bmatrix} V_\alpha \\ V_\beta \end{bmatrix} \end{aligned} \tag{24}$$

Substituting the constraint condition into the cost function, the unconstrained optimization problem is presented in (25).

$$\min f_2 = \|\mathbf{T}\|_2 = (t_c + a)^2 + (t_c + b)^2 + {t_c}^2 \tag{25}$$

The first derivative of f_2 is deduced as

$${f_2}' = 2(t_c + a) + 2(t_c + b) + 2t_c. \tag{26}$$

The minimum value occurs in ${f_2}' = 0$. Thus, the optimal dwell time can be deduced as shown in (27).

$$\begin{cases} \tau_{c2} = -\frac{a+b}{3} \\ \tau_{a2} = -\frac{a+b}{3} + a \\ \tau_{b2} = -\frac{a+b}{3} + b \end{cases} \tag{27}$$

According to (27), the SVPWM with the OVDT of the 2-norm needs to generate three nonzero vectors in one PWM period. However, the general center-aligned PWM signal only can generate two nonzero vectors in one period. To generate three nonzero vectors, phase-shift PWM is utilized.

From (27), the relationship among τ_{a2}, τ_{b2}, and τ_{c2} can be deduced as

$$\tau_{a2} + \tau_{b2} + \tau_{c2} = 0. \tag{28}$$

From (28), τ_{a2}, τ_{b2}, and τ_{c2} will not have the same plus-minus sign. According to the plus-minus sign, phase-shift PWM can be divided into six cases, which are presented in Figure 7.

In case 1, the reference vector is composed of $\mathbf{V_a}$, $-\mathbf{V_b}$, and $-\mathbf{V_c}$. The duty cycle can be deduced as shown in (29).

$$\begin{cases} d_{a2} = \frac{\tau_{a2} - \tau_{b2} - \tau_{c2} + t_7}{T_s} = \frac{\tau_{a2} - \tau_{b2} - \tau_{c2}}{2T_s} + \frac{1}{2} \\ d_{b2} = \frac{-\tau_{c2} + t_7}{T_s} = \frac{\tau_{b2} - \tau_{b2} - \tau_{c2}}{2T_s} + \frac{1}{2} \\ d_{c2} = \frac{-\tau_{b2} + t_7}{T_s} = \frac{\tau_{c2} - \tau_{b2} - \tau_{c2}}{2T_s} + \frac{1}{2} \end{cases} \tag{29}$$

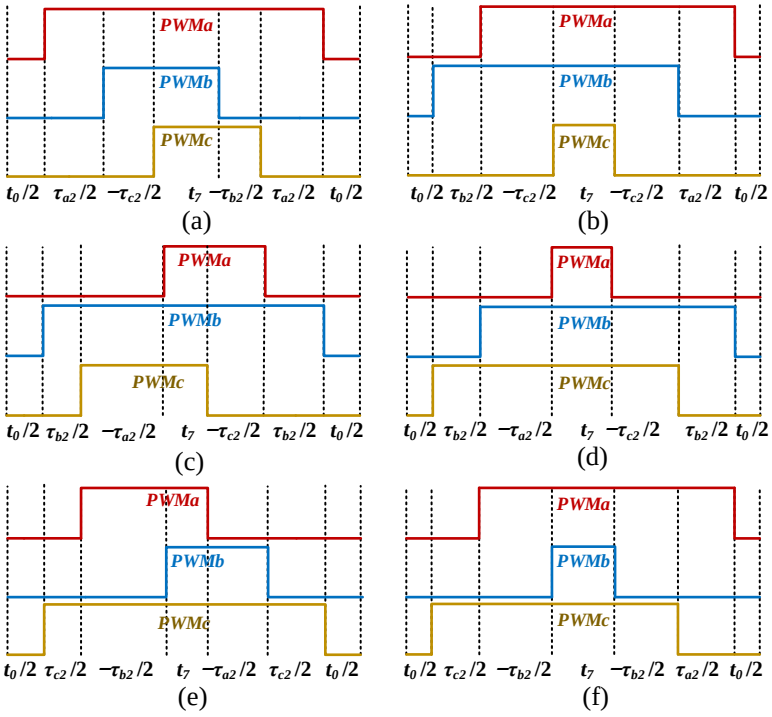

Figure 7. The phase-shift PWM signal: (**a**) case 1: $\tau_{a2} > 0$, $\tau_{b2} < 0$, and $\tau_{c2} \leq 0$, (**b**) case 2: $\tau_{a2} > 0$, $\tau_{b2} > 0$, and $\tau_{c2} \leq 0$, (**c**) case 3: $\tau_{a2} \leq 0$, $\tau_{b2} > 0$, and $\tau_{c2} < 0$, (**d**) case 4: $\tau_{a2} \leq 0$, $\tau_{b2} > 0$, and $\tau_{c2} > 0$, (**e**) case 5: $\tau_{a2} < 0$, $\tau_{b2} \leq 0$, and $\tau_{c2} > 0$, (**f**) case 6: $\tau_{a2} > 0$, $\tau_{b2} \leq 0$, and $\tau_{c2} > 0$.

PWMb and PWMc must have a phase difference, as shown in Figure 8a. The phase difference between PWMb and PWMc can be deduced as

$$t_{bc} = T_s d_{b2} - t_d - t_7 \tag{30}$$

where t_d is presented as

$$t_d = \frac{T_s d_{b2} - T_s d_{a2}}{2}. \tag{31}$$

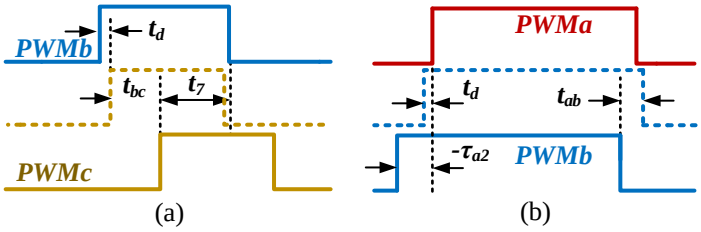

Figure 8. The relationship of the phase differences. (**a**) $\tau_{a2} > 0$, $\tau_{b2} < 0$, and $\tau_{c2} \leq 0$, (**b**) $\tau_{a2} \leq 0$, $\tau_{b2} > 0$, and $\tau_{c2} > 0$.

Substituting (31) into (30), t_{bc} can be deduced as

$$t_{bc} = \frac{\tau_{b2} + \tau_{c2}}{2}. \tag{32}$$

To obtain the phase difference of (32), the phase shift of PWMb is set as $-\tau_{c2}/2$, the phase shift of PWMc is set as $-\tau_{b2}/2$, and the phase shift of PWMa is set as zero. The calculated expression of the phase shift is deduced as

$$\begin{cases} p_a = 0 \\ p_b = \frac{-\tau_{c2}}{2T_s} \\ p_c = \frac{-\tau_{b2}}{2T_s} \end{cases}. \tag{33}$$

In case 2, the reference vector is composed of $\mathbf{V_a}$, $\mathbf{V_b}$, and $-\mathbf{V_c}$. The duty cycle can be deduced to be the same as (29). PWMa and PWMb should have a phase difference, as presented in Figure 8b. The phase difference can be deduced as

$$t_{ab} = \tau_{a2} - t_d = \tau_{a2} - d_{b2}T_s - d_{a2}T_s = \frac{\tau_{a2} + \tau_{b2}}{2}. \tag{34}$$

To obtain the phase difference of (34), the phase shift of PWMa is set as zero, and the phase shift of PWMb is set as $(\tau_{a2} + \tau_{b2})/2$. According to (28), the phase shift of PWMb can be further deduced as $-\tau_{c2}/2$. To obtain the same calculation expression as that of (33), the phase shift of PWMc is set as $-\tau_{b2}/2$.

It can be deduced that the duty cycle and phase shift calculated expressions of the six cases of Figure 7 are the same. Combining (27), (29), and (33), the duty cycle and phase shift calculated expressions can be deduced as (35) and (36), respectively.

$$\begin{cases} d_{a2} = -\frac{(a+b)}{3T_s} + \frac{1}{2} \\ d_{b2} = \frac{2a-b}{3T_s} + \frac{1}{2} \\ d_{c2} = \frac{2b-a}{3T_s} + \frac{1}{2} \end{cases} \tag{35}$$

$$\begin{cases} p_{a2} = 0 \\ p_{b2} = \frac{a+b}{6} \\ p_{c2} = \frac{2b-a}{6} \end{cases} \tag{36}$$

The duty cycle and phase shift in one period are shown in Figure 9. From (35) and (36), the SVPWM algorithm with the OVDT of the 2-norm can directly calculate the duty cycle and phase shift without a logical judgment. Compared with the conventional SVPWM algorithm, the SVPWM algorithm with the OVDT of the 2-norm is extremely simplified.

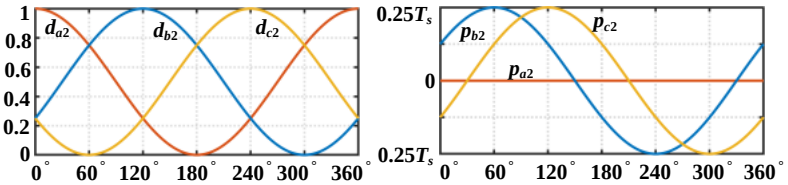

Figure 9. (**a**) The duty cycle in one period. (**b**) The phase shift in one period.

The flowcharts of the conventional SVPWM algorithm and the proposed SVPWM algorithm with the OVDTs of the 1-norm and the 2-norm are shown in Figure 10. According to Figure 10a, the conventional SVPWM algorithm needs to identify the sector by calculating the sector index. Then, the duty cycles are calculated according to the identified sector. The sector identification and duty cycle calculation need logical judgments and multiply-accumulate calculations. From Figure 10b,c, the proposed SVPWM algorithm does not need sector identification. The SVPWM algorithm with the OVDT of the 1-norm only needs some logical judgments. Then, the duty cycles can be calculated by Equation (21). The proposed SVPWM algorithm with the OVDT of the 2-norm needs no logical judgment. The duty cycle and phase shift can be calculated by using Equations (35) and (36). Compared to the conventional SVPWM algorithm, the proposed SVPWM algorithm has a more concise calculation process that needs fewer multiply-accumulate calculations and logical

judgments. Thus, the computational complexity of the proposed SVPWM algorithm is reduced and the proposed SVPWM algorithm is simpler.

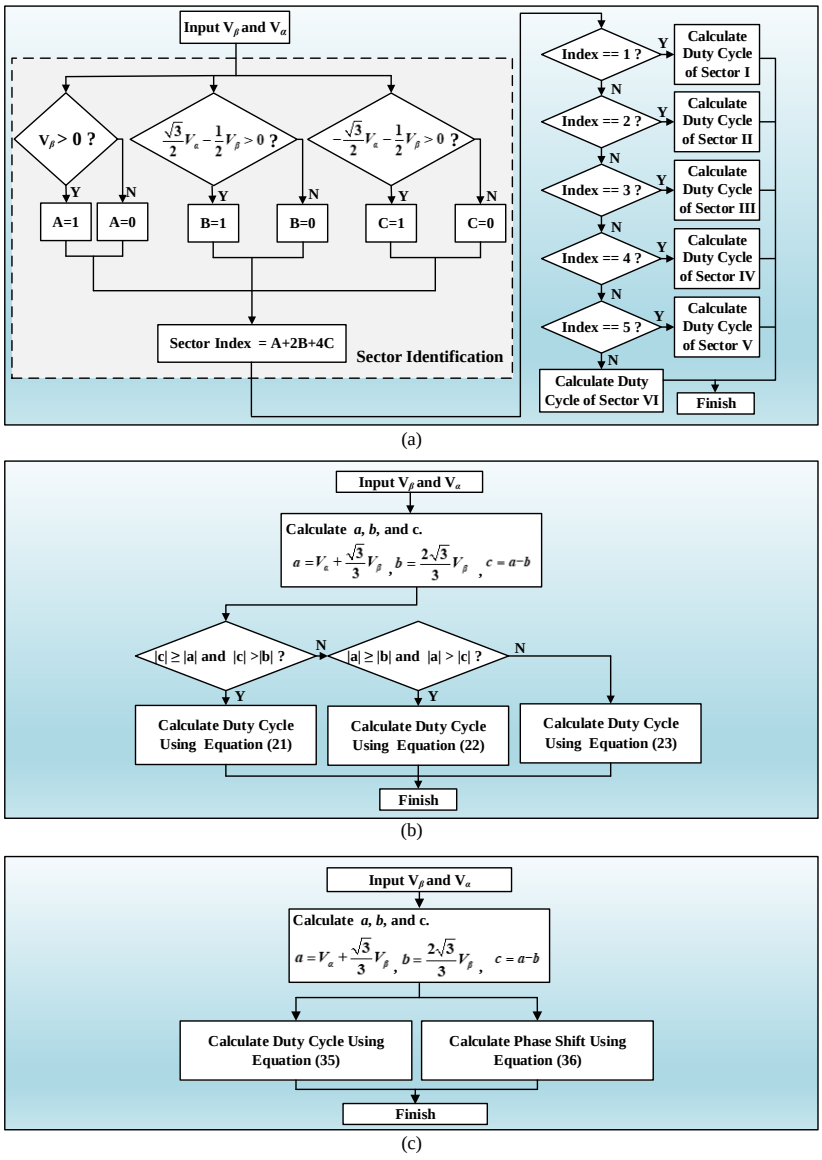

Figure 10. (**a**) The flowchart of the conventinal SVPWM algorithm. (**b**) The flowchart of the proposed SVPWM algorithm with the OVDT of the 1-norm. (**c**) The flowchart of the proposed SVPWM algorithm with the OVDT of the 2-norm.

4. Experimental Results

To verify the proposed SVPWM algorithm with the OVDT, corresponding experiments are performed in a 36,000 rpm FESS prototype. The proposed SVPWM algorithm is implemented in a PMSM FOC system to verify that the algorithm can convert the DC to AC. Additionally, the time consumption of the proposed SVPWM algorithm, conventional SVPWM algorithm, max-min SVPWM algorithm [17], and third harmonic injection SVPWM algorithm [31] are compared to verify that the proposed SVPWM algorithm is simpler. Furthermore, a case for increasing the sampling frequency by using simplified SVPWM is presented. With the sampling frequency increasing, the current THD and eddy current loss can be reduced.

4.1. Experimental Setup

The experimental platform is shown in Figure 11, which mainly includes an FESS prototype, a PMSM drive, a magnetic levitation controller, an oscilloscope, a power analyzer, and PCs. The FESS prototype and its structure schematic drawing are shown in Figure 12. The specifications of the FESS prototype are listed in Table 1. The FESS prototype has a 32 kg metal flywheel rotor, which can store 357 Wh energy. The flywheel rotor connects to the rotor of the PMSM. The flywheel rotor will have the same rotation speed as the rotor of the PMSM. The PMSM applied in the FESS is presented in Figure 13. A four-pole rotor is employed in the PMSM. The rotor utilizes a permanent magnet (PM) Halbach array to obtain a sinusoidal back EMF. The PM Halbach array is bound with carbon fiber to obtain high strength. The PMSM utilizes toroidal winding and slotless structure in the stator. Soft magnetic ferrite is employed in the stator to obtain low eddy current loss. The main specifications of the PMSM are listed in Table 2. The machine driver constitutes an MCU of TMS320F28379D and SiC MOSFET IM828MCC. Active magnetic bearings with the controller are applied to brace the flywheel rotor, which flywheel rotor can operate at a high rotation speed without friction. The experimental platform also possesses the Tektronix oscilloscope and HIOKI power analyzer to analyze the corresponding signals.

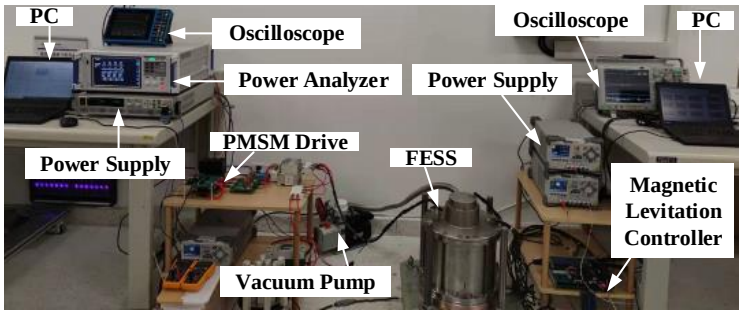

Figure 11. The experimental platform of the 8 kW FESS prototype.

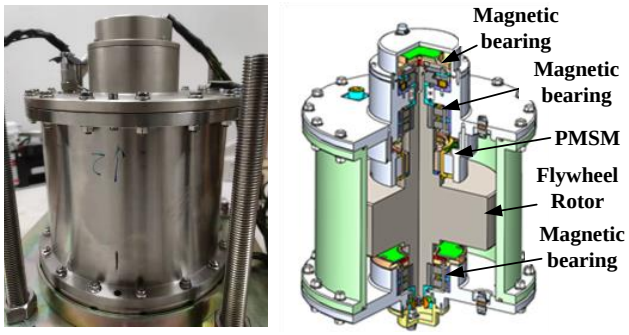

Figure 12. The prototype of the 8 kW FESS.

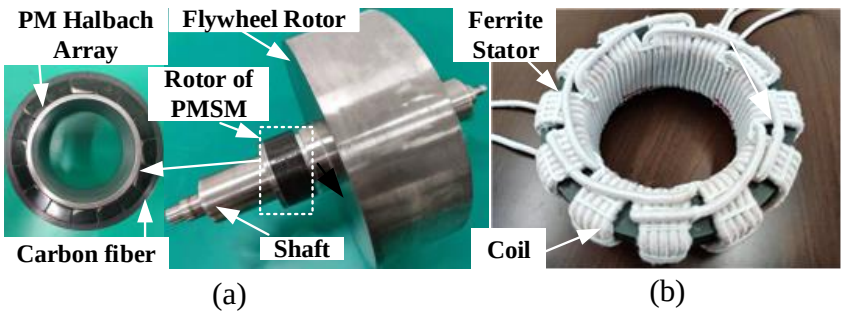

Figure 13. The PMSM of the FESS. (**a**) The rotor. (**b**) The stator.

Table 1. The main specifications of the FESS prototype.

Symbol	Description	Value
V_{AC}	Output voltage	110 V
P_r	Maximum power	8 kW
E	Stored energy	357.3 Wh
ω_m	Maximum speed	36,000 rpm
M_r	Rotor weight	32.5 kg
S_m	Prototype size	Φ350 × 420 mm

Table 2. The main specifications of the PMSM.

Symbol	Description	Value
P_r	Maximum power	8 kW
V	Rated voltage	110 VAC
ω_m	Maximum speed	36,000 rpm
P	Number of poles	4
L_s	Stator inductance	14 μH
R_s	Stator resistance	8 mΩ

4.2. Application to FOC

The proposed SVPWM algorithm is applied to the PMSM FOC to verify it can convert the DC to AC. The PMSM FOC block diagram is presented in Figure 14. The inputs of the SVPWM algorithm are $\mathbf{V}_\alpha$ and $\mathbf{V}_\beta$, which are generated by the proportional–integral (PI) controller and inverse Park transform. The outputs of the SVPWM algorithm are the duty cycles. The three-phase inverter can convert DC to AC according to the duty cycles generated by the SVPWM algorithm.

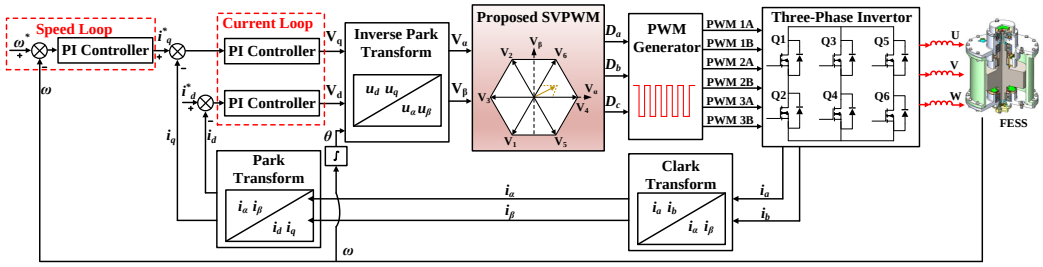

Figure 14. The block diagram of the proposed SVPWM algorithm implemented in PMSM FOC.

The SVPWM method with the OVDT of the 1-norm is implemented in the FOC system. The PWM signal of the SVPWM algorithm with the OVDT of the 1-norm is shown in Figure 15. The PWM signal with the OVDT of the 1-norm is a center-aligned signal, which is the same as the conventional SVPWM algorithm because those two algorithms both compose the reference vector using two adjacent vectors. In Figure 15, the reference vector is composed of the adjacent vectors of $\mathbf{V_4}$ and $\mathbf{V_6}$. When the PMSM operates at 30,000 rpm, the three-phase current is as shown in Figure 16a. A sinusoidal three-phase current is obtained by using SVPWM with the OVDT of the 1-norm. Fourier analysis is performed through the power analyzer. The frequency spectrum of the phase current is shown in Figure 16b. The fundamental frequency is 1 kHz. The three-phase current has high-frequency harmonics of 40 kHz and 80 kHz, which are caused by the switching of the SiC MOSFET. The current also has 3rd and 5th harmonics, which are caused by the harmonics of the back electromotive force (EMF). The THD of the phase current is smaller than 0.084. The experimental results show that the SVPWM algorithm with the OVDT of the 1-norm can be effectively implemented in the FOC of the PMSM.

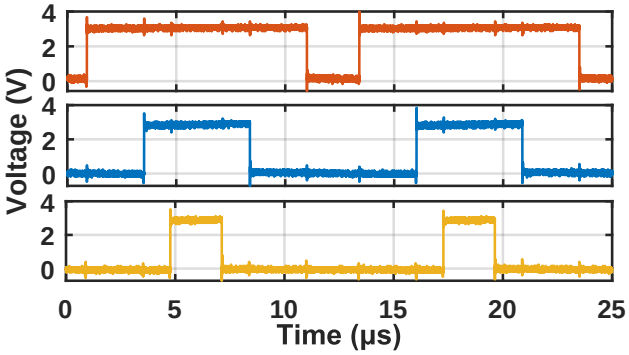

Figure 15. The PWM signal of the SVPWM algorithm with OVDT of 1-norm.

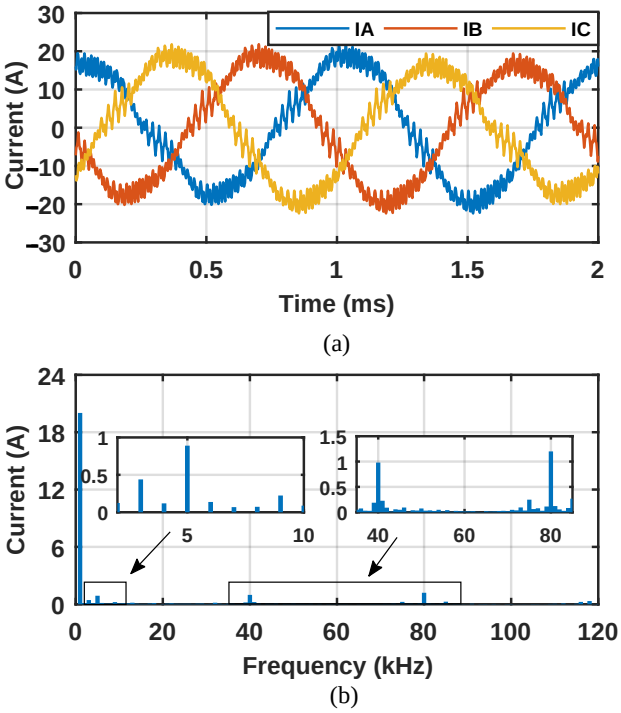

Figure 16. The current of the SVPWM algorithm with OVDT of 1-norm. (**a**) The three-phase current. (**b**) The harmonic of the current.

Similarly, the SVPWM algorithm with the OVDT of the 2-norm is implemented in the PMSM FOC system. The PWM signal of the SVPWM algorithm with the OVDT of the 2-norm is shown in Figure 17. The PWM signal with the OVDT of the 2-norm is not center-aligned, which is different from the conventional SVPWM algorithm. The reference vector is composed using three nonzero vectors. In Figure 17, the reference vector is composed of $\mathbf{V_4}$, $\mathbf{V_5}$, and $\mathbf{V_6}$. The PMSM also operates at 30,000 rpm. The three-phase current is shown in Figure 18a. The frequency spectrum of the current is shown in Figure 18b. The phase current also has a 40 kHz, 80 kHz, 3rd, and 5th harmonic. The THD of the current is smaller than 0.093. As mentioned above, the SVPWM algorithm with the OVDT of the 2-norm is simpler than the algorithm with the OVDT of the 1-norm. However, the PWM signal of the SVPWM algorithm of the 2-norm is asymmetric. Thus, the current THD of the SVPWM algorithm of the 2-norm will be larger than the SVPWM algorithm of the 1-norm.

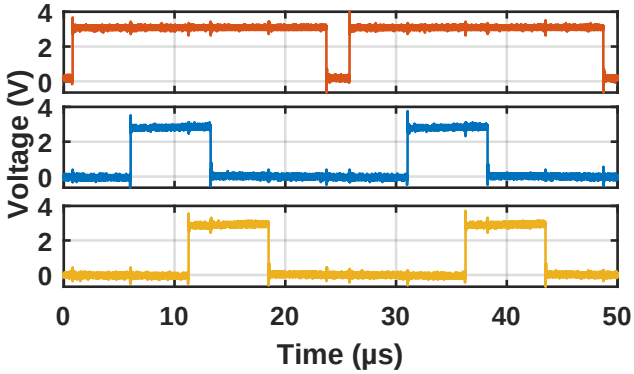

Figure 17. The PWM signal of the SVPWM algorithm with the OVDT of the 2-norm.

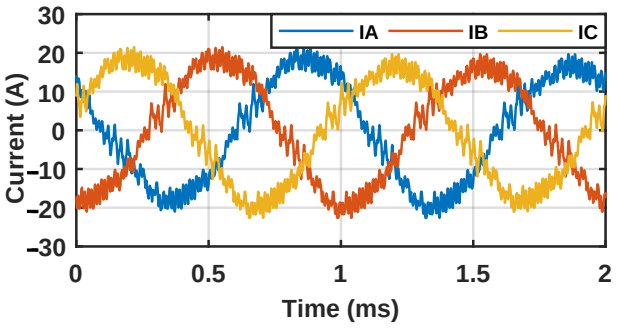

(a)

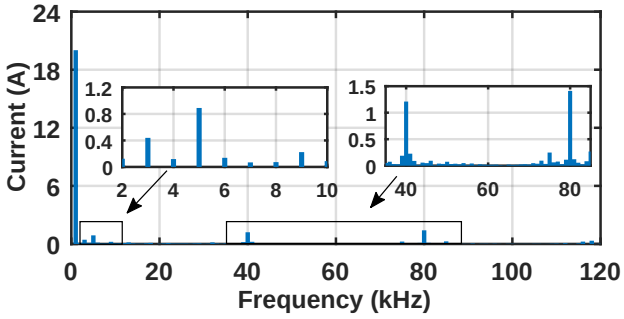

(b)

Figure 18. The current of the SVPWM algorithm with the OVDT of the 2-norm. (**a**) The three-phase current. (**b**) The harmonic of the current.

The experimental results show that the SVPWM algorithm with the OVDTs of the 1-norm and the 2-norm can be implemented in the PMSM FOC system to achieve a THD smaller than 9.3%. The efficiency of the proposed SVPWM algorithm with the OVDT is thus verified.

4.3. Execution Time of the SVPWM Algorithm

To verify that the proposed SVPWM algorithm is simpler, the execution time of the proposed SVPWM algorithm, conventional SVPWM algorithm, SVPWM algorithm without sector identification [17], SVPWM algorithm with fast sector identification [18], and third-harmonic injection SVPWM algorithm [31] are presented. For a fair comparison, the SVPWM algorithms are implemented in the commonly used MCUs. The commonly used MCUs include Texas Instruments TMS320F28379D, STMicroelectronics STM32F405, and STM32F103. The TMS320F28379D, STM32F405, and STM32F103 operate at frequencies of 150 MHz, 140 MHz, and 72 MHz, respectively. For the TMS320F28379D, the compiler CCS9.0.1 is utilized. For the STM32F405 and STM32F103, the compiler Keil uVision 5 is utilized. The program of the algorithm is respectively executed in two conditions. One condition is that the program runs in the flash of the MCU, and the data type of the pro-

gram adopts IEEE 754 floating-point type. The other condition is the optimized condition, in which the program runs in the RAM of the MCU and the IQmath library is used to avoid floating point calculation. The emulators Texas Instruments XDS100V2 and STMicroelectronics ST-LINKV2 are used to measure the execution times and processor cycles of the SVPWM algorithms.

The experimental results of the execution times and processor cycles of the SVPWM algorithms are listed in Table 3. The experimental results show that the execution time can be reduced by running the program in the RAM and using the IQmath library because the data read-and-write cycles in the flash are longer than in the RAM. The execution time also can be reduced by using the IQmath library to avoid floating point calculation. Especially in the STM32F103, which has no floating-point processing unit (FPU), the execution time can be significantly reduced by using the IQmath library. In the same condition, the proposed SVPWM algorithm spends less time than the conventional SVPWM algorithm. The simplified SVPWM algorithm in [17] does not need sector identification to calculate the duty cycles, which is similar to the proposed SVPWM with the OVDT of the 1-norm. Thus, the execution time of those two algorithms is similar. The simplified SVPWM algorithm in [18] can achieve fast sector identification. Therefore, it can spend less time than the conventional SVPWM algorithm. However, it will spend more time than the proposed SVPWM with the OVDT of the 1-norm. The proposed SVPWM algorithm with the OVDT of the 2-norm and the SVPWM algorithm in [31] do not need logical judgments to calculate the duty cycles. Therefore, they show lower time consumption than the other SVPWM algorithms. However, the SVPWM algorithm in [31] needs to address the trigonometric function. Thus, the proposed SVPWM algorithms with the OVDT of the 2-norm require the least time among the SVPWM algorithms.

Table 3. Execution time of the SVPWM algorithms.

MCU Types	SVPWM Algorithms	Execution Time @ Flash @ Floating Point	Processor Cycles @ Flash @ Floating Point	Execution Time @ RAM @IQmath Library	Processor Cycles @ RAM @IQmath Library
TMS320 F28379D	SVPWM algorithm with the OVDT of the 1-norm	8.2 µs	1229	2.6 µs	390
	SVPWM algorithm with the OVDT of the 2-norm	6.3 µs	945	1.9 µs	285
	Conventional SVPWM algorithm	13.4 µs	2008	4.2 µs	629
	SVPWM algorithm in [17]	8.5 µs	1274	2.7 µs	404
	SVPWM algorithm in [18]	10.2 µs	1592	3.4 µs	510
	SVPWM algorithm in [31]	7.4 µs	1109	2.3 µs	344
STM32 F405	SVPWM algorithm with the OVDT of the 1-norm	9.7 µs	1358	3.0 µs	420
	SVPWM algorithm with the OVDT of the 2-norm	7.1 µs	994	2.2 µs	308
	Conventional SVPWM algorithm	15.2 µs	2128	5.3 µs	742
	SVPWM algorithm in [17]	9.8 µs	1372	3.1 µs	434
	SVPWM algorithm in [18]	11.6 µs	1642	3.7 µs	518
	SVPWM algorithm in [31]	8.1 µs	1134	2.5 µs	350
STM32 F103	SVPWM algorithm with the OVDT of the 1-norm	45.8 µs	3297	9.2 µs	662
	SVPWM algorithm with the OVDT of the 2-norm	35.2 µs	2640	6.7 µs	482
	Conventional SVPWM algorithm	73.5 µs	5292	14.1 µs	1015
	SVPWM algorithm in [17]	46.3 µs	3334	9.6 µs	691
	SVPWM algorithm in [18]	64.5 µs	4644	11.7 µs	824
	SVPWM algorithm in [31]	40.3 µs	2901	7.8 µs	561

4.4. Increasing Sampling Frequency by Using Simplified SVPWM Algorithm

In this paper, the purpose of the simplified SVPWM algorithm is to increase the sampling frequency of the control system. A case that increases the sampling frequency using the proposed SVPWM algorithm with the OVDT of the 1-norm is presented. The program of the FOC runs in the flash, and the data type of the program adopts IEEE 754 floating-point type.

The PMSM FOC mainly includes A/D conversion, position decoding, coordinate transformation, the calculation of the control law, and SVPWM. The execution time of each part of the FOC is shown in Figure 19. The sampling frequency of the FOC with the conventional SVPWM algorithm is 33 kHz. The sampling frequency can increase to 40 kHz by using the proposed SVPWM algorithm with the OVDT of the 1-norm. The currents of the proposed and conventional SVPWM algorithms are shown in Figure 20a,b. The frequency spectrum of the current is shown in Figure 20c. The current THDs of the FOC with the proposed and conventional SVPWM algorithms are 0.084 and 0.113, respectively. The current THD can be reduced by 25.6% by using the proposed SVPWM algorithm.

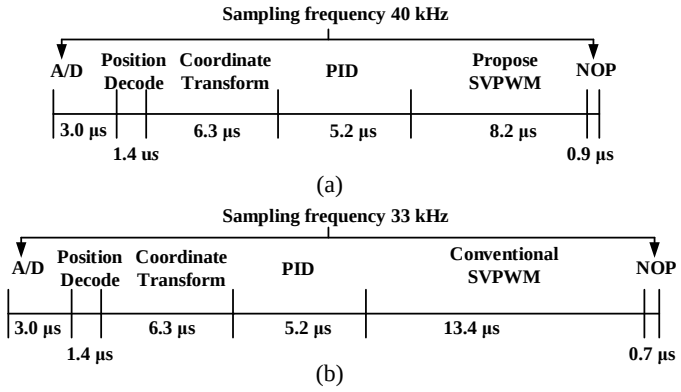

Figure 19. (**a**) Time consumption of the FOC with proposed SVPWM algorithm. (**b**) Time consumption of the FOC with conventional SVPWM algorithm.

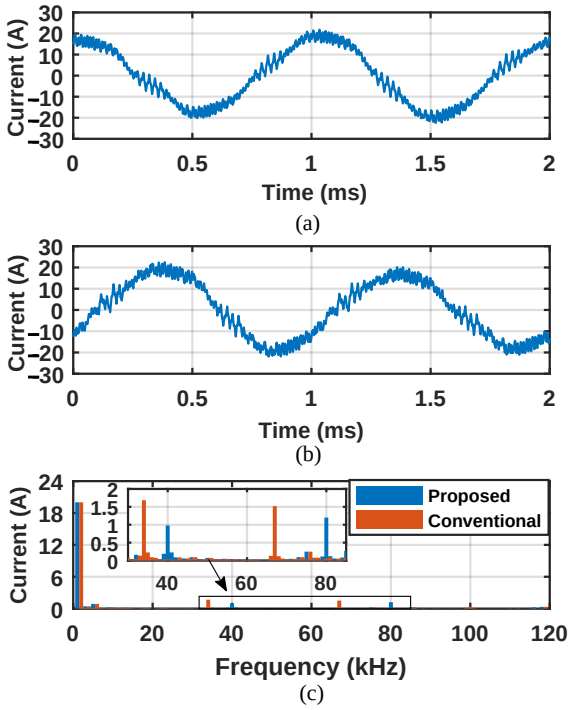

Figure 20. The phase current. (**a**) The phase current of proposed SVPWM algorithm. (**b**) The phase current of conventional SVPWM algorithm. (**c**) The harmonic of the current.

The current THD will cause eddy current loss of the PMSM, which will influence the maintenance speed power consumption of the FESS. The maintenance speed power consumption with the proposed and conventional SVPWM algorithms is shown in Figure 21. The maintenance speed power consumption with the conventional SVPWM algorithm is 64.5 W. The maintenance speed power consumption of the proposed SVPWM algorithm is 61.8 W, which is reduced by 4.1%. The experimental results show that the FESS requires less power consumption to maintain the flywheel rotor speed by using the proposed SVPWM algorithm.

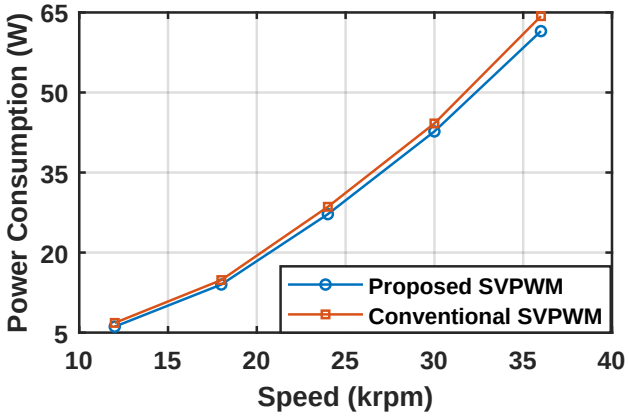

Figure 21. The maintenance speed power consumption of the proposed and conventional SVPWM algorithm.

5. Conclusions

In this paper, a new simplified SVPWM algorithm with the OVDT is proposed from the perspective of optimization. The theoretical derivation and algorithm flow of the SVPWM algorithm with the OVDTs of the 1-norm and 2-norm is presented. Then, the proposed SVPWM algorithm is implemented in a high-speed PMSM drive of FESS. The execution time of the proposed SVPWM algorithm, conventional SVPWM algorithm, and SVPWM algorithms from [17,18,31] are compared. Finally, a case that increases the sampling frequency by using the proposed simplified SVPWM algorithm is presented. The main conclusion is drawn as follows:

(1) In the proposed SVPWM algorithm, the vector dwell time can be directly calculated by solving the optimization problem without sector identification. Compared with the conventional SVPWM algorithm, the proposed SVPWM algorithm needs less equation expression and logical judgment. Thus, the proposed SVPWM algorithm is simpler.
(2) The proposed SVPWM algorithm is implemented in an FESS prototype. The experimental results show that the proposed SVPWM algorithm can generate a three-phase sinusoidal current for the PMSM of the FESS. The current THD can be smaller than 9.3% at the speed of 30,000 rpm.
(3) Compared to the conventional SVPWM algorithm, the time consumption of the proposed SVPWM algorithm is reduced. With the time consumption reduced, a higher sampling frequency of the control system can be obtained. The current THD and eddy current loss can be reduced by increasing the sampling frequency. As a result, the maintenance speed power consumption is reduced by 4.1% through using the proposed SVPWM algorithm.

6. Future Work

In this paper, a new simplified SVPWM algorithm is presented, and the proposed SVPWM algorithm shows some superiority. However, there are still some limitations to the proposed SVPWM algorithm. The limitations and future work of the proposed SVPWM algorithm are presented as follows:

(1) The proposed SVPWM algorithm is only implemented in a PMSM FOC with a sampling frequency of 40 kHz. The execution time can be further reduced by running the program in the RAM and using the IQmath library. The proposed SVPWM algorithm is expectantly utilized in a higher-sampling-frequency PMSM FOC system, such as a 100 kHz FOC system.
(2) The FESS is generally utilized in a high-power application. The power of the FESS of this paper is relatively low. In future work, the proposed SVPWM algorithm may be applied in a higher-power FESS. In high-power FESS, the influence of the SVPWM algorithm on thermal and efficiency can be an appropriate analysis because the problem of thermal and efficiency is notable in high-power FESS.
(3) The proposed SVPWM algorithm deduces the dwell time of the basic vector from the perspective of optimization, which shows a more concise process compared to the conventional SVPWM algorithm. However, the proposed SVPWM algorithm only can apply to the commonly used three-phase two-level DC/AC converter. The multiphase PMSM and multilevel converter have received increasing attention in recent years [33–35]. The proposed SVPWM algorithm can be extended to the multiphase and multilevel DC/AC converter.

Author Contributions: Conceptualization, K.L.; Data curation, X.S.; Funding acquisition, K.L.; Investigation, H.H. and H.W.; Methodology, H.H.; Software, J.W.; Validation, H.W. and J.W.; Writing—original draft, H.H.; Writing—review & editing, H.W. and J.W. All authors have read and agreed to the published version of the manuscript.

Funding: Technology program of Shenzhen China under Grants JCYJ20200109142205924, 202001093000459.

Institutional Review Board Statement: Not applicable.

Informed Consent Statement: Not applicable.

Data Availability Statement: The data presented in this study are available on request from the corresponding author. The data are not publicly available due to the privacy agreement among co-authors.

Conflicts of Interest: The authors declare no conflict of interest.

Nomenclature

$\mathbf{V_r}$	Reference vector
$\mathbf{V}_\alpha$, $\mathbf{V}_\beta$	Projection of $\mathbf{V_r}$ on the α and β axes
$\mathbf{V_0}$, $\mathbf{V_1}$, $\mathbf{V_2}$, $\mathbf{V_3}$, $\mathbf{V_4}$, $\mathbf{V_5}$, $\mathbf{V_6}$, $\mathbf{V_7}$	Basic vectors of the PMSM drive
$\mathbf{V_a}$, $\mathbf{V_b}$, $\mathbf{V_c}$	Redefined basic vectors
T_s	The period of the PWM signal
t_0, t_4, t_6, t_7	Dwell time of $\mathbf{V_0}$, $\mathbf{V_4}$,$\mathbf{V_6}$, and $\mathbf{V_7}$
t_a, t_b, t_c	Dwell time of $\mathbf{V_a}$,$\mathbf{V_b}$, and $\mathbf{V_c}$
f_1,f_2	Cost functions of the 1-norm and 2-norm
$f_1{}'$, $f_2{}'$	First derivative of f_1 and f_2
$f_1{}''$, $f_2{}''$	Second derivative of f_2 and f_2
τ_{a1}, τ_{b1}, τ_{c1}	Optimal vector dwell time of the 1-norm
τ_{a2}, τ_{b2}, τ_{c2}	Optimal vector dwell time of the 2-norm
d_{a1}, d_{b1}, d_{c1}	Duty cycles of the SVPWM algorithm with the OVDT of the 1-norm
d_{a2}, d_{b2}, d_{c2}	Duty cycles of the SVPWM algorithm with the OVDT of the 2-norm
p_{a2}, p_{b2}, p_{c2}	Phase shifts of the SVPWM algorithm with the OVDT of the 2-norm
sgn	Sign function
δ	Dirac delta function

References

1. Olabi, A.G.; Wilberforce, T.; Abdelkareem, M.A.; Ramadan, M. Critical Review of Flywheel Energy Storage System. *Energies* **2021**, *14*, 2159. [CrossRef]
2. Zhang, W.; Wang, J.; Zhu, P.; Yu, J. A Novel Vehicle-Mounted Magnetic Suspension Flywheel Battery with a Virtual Inertia Spindle. *IEEE Trans. Ind. Electron.* **2021**, *69*, 5973–5983. [CrossRef]
3. Zhang, W.; Li, Y.; Wu, G.; Rao, Z.; Gao, J.; Luo, D. Robust Predictive Power Control of *N**3-Phase PMSM for Flywheel Energy Storage Systems Application. *Energies* **2021**, *14*, 3684. [CrossRef]
4. Haidl, P.; Buchroithner, A. Design of a Low-Loss, Low-Cost Rolling Element Bearing System for a 5 kWh/100 kW Flywheel Energy Storage System. *Energies* **2021**, *14*, 7195. [CrossRef]
5. Masouleh, M.I.; Limebeer, D.J. Fuel Minimization for a Vehicle Equipped with a Flywheel and Battery on a Three-Dimensional Track. *IEEE Trans. Intell. Veh.* **2017**, *2*, 161–174. [CrossRef]
6. Ershad, N.F.; Mehrjardi, R.T.; Ehsani, M. High-performance 4wd Electric Powertrain with Flywheel Kinetic Energy Recovery. *IEEE Trans. Power Electron.* **2020**, *36*, 772–784. [CrossRef]
7. Canova, A.; Campanelli, F.; Quercio, M. Flywheel Energy Storage System in Italian Regional Transport Railways: A Case Study. *Energies* **2022**, *15*, 1096. [CrossRef]
8. Jia, Y.; Wu, Z.; Zhang, J.; Yang, P.; Zhang, Z. Control Strategy of Flywheel Energy Storage System Based on Primary Frequency Modulation of Wind Power. *Energies* **2022**, *15*, 1850. [CrossRef]
9. Mukoyama, S.; Nakao, K.; Sakamoto, H.; Matsuoka, T. Development of Superconducting Magnetic Bearing for 300 kW Flywheel Energy Storage System. *IEEE Trans. Appl. Supercond.* **2017**, *27*, 1–4. [CrossRef]
10. Ghanaatian, M.; Lotfifard, S. Control of Flywheel Energy Storage Systems in the Presence of Uncertainties. *IEEE Trans. Sustain. Energy* **2018**, *10*, 36–45. [CrossRef]
11. Werfel, F.N.; Floegel-Delor, U.; Riedel, T. A Compact HTS 5 kWh/250 kW Flywheel Energy Storage System. *IEEE Trans. Appl. Supercond.* **2007**, *17*, 2138–2141. [CrossRef]
12. Gengji, W.; Ping, W. Rotor Loss Analysis of PMSM in Flywheel Energy Storage System as Uninterruptable Power Supply. *IEEE Trans. Appl. Supercond.* **2016**, *26*, 1–5. [CrossRef]
13. Ji, W.; Ni, F.; Gao, D.; Luo, S.; Lv, Q.; Lv, D. Electromagnetic Design of High-Power and High-Speed Permanent Magnet Synchronous Motor Considering Loss Characteristics. *Energies* **2021**, *14*, 3622. [CrossRef]
14. Jarzebowicz, L. Errors of a Linear Current Approximation in High-Speed PMSM Drives. *IEEE Trans. Power Electron.* **2017**, *32*, 8254–8257. [CrossRef]
15. Zhang, X.; Chen, Y.; Mollet, Y.; Yang, J.; Gyselinck, J. An Accurate Discrete Current Controller for High-Speed PMSMs/Gs in Flywheel Applications. *Energies* **2020**, *13*, 1458. [CrossRef]
16. Ullah, K.; Guzinski, J.; Mirza, A.F. Critical Review on Robust Speed Control Techniques for Permanent Magnet Synchronous Motor (PMSM) Speed Regulation. *Energies* **2022**, *15*, 1235. [CrossRef]
17. Chung, D.W.; Kim, J.S.; Sul, S.K. Unified Voltage Modulation Technique for Real-Time Three-Phase Power Conversion. *IEEE Trans. Ind. Appl.* **1998**, *34*, 374–380. [CrossRef]
18. Shu, Z.; Tang, J.; Guo, Y.; Lian, J. An Efficient SVPWM Algorithm with Low Computational Overhead for Three-Phase Inverters. *IEEE Trans. Power Electron.* **2007**, *22*, 1797–1805. [CrossRef]
19. Yu, B.; Song, W.; Guo, Y. A Simplified and Generalized SVPWM Scheme for Two-Level Multiphase Inverters with Common-Mode Voltage Reduction. *IEEE Trans. Ind. Electron.* **2021**, *69*, 1378–1388. [CrossRef]
20. Ni, K.; Hu, Y.; Liu, Y.; Gan, C. Performance Analysis of a Four-Switch Three-Phase Grid-Side Converter with Modulation Simplification in a Doubly-Fed Induction Generator-Based Wind Turbine (DFIG-WT) with Different External Disturbances. *Energies* **2017**, *10*, 706. [CrossRef]
21. Alouane, A.; Rhouma, A.B.; Hamouda, M.; Khedher, A. Efficient FPGA-Based Real-Time Implementation of an SVPWM Algorithm for a Delta Inverter. *IET Power Electron.* **2018**, *11*, 1611–1619. [CrossRef]
22. Ma, H.; Lu, Y.; Zheng, K.; Xu, T. Research on the Simplified SVPWM for Three-Phase/Switches Y-Type Two-Level Rectifier. *IEEE Access* **2020**, *8*, 214310–214321. [CrossRef]
23. Yan, Q.; Zhou, Z.; Wu, M.; Yuan, X. A Simplified Analytical Algorithm in abc Coordinate for the Three-Level SVPWM. *IEEE Trans. Power Electron.* **2020**, *36*, 3622–3627. [CrossRef]
24. Hu, J.S.; Lin, J.N.; Chen, H.C. A Discontinuous Space Vector PWM Algorithm in abc Reference Frame for Multilevel Three-Phase Cascaded H-Bridge Voltage Source Inverters. *IEEE Trans. Ind. Electron.* **2017**, *64*, 8406–8414. [CrossRef]
25. Jacob, B.; Baiju, M.R. A New Space Vector Modulation Scheme for Multilevel Inverters Which Directly Vector Quantize the Reference Space Vector. *IEEE Trans. Ind. Electron.* **2014**, *62*, 88–95. [CrossRef]
26. Szczepankowski, P.; Nieznański, J. Application of Barycentric Coordinates in Space Vector PWM Computations. *IEEE Access* **2019**, *7*, 91499–91508. [CrossRef]
27. Wang, Q.; Chen, P.; Deng, F.; Cheng, M.; Buja, G. A Novel Method Simulating Human Eye Recognition for Sector Judgement of SVPWM Algorithm. *IEEE Access* **2020**, *8*, 90216–90224. [CrossRef]
28. Bose, B.K. Neural Network Applications in Power Electronics and Motor Drives—An Introduction and Perspective. *IEEE Trans. Ind. Electron.* **2007**, *54*, 14–33. [CrossRef]

29. Langer, N.; Bhat, A.H.; Agarwal, P. Neural-Network-Based Space-Vector Pulse-Width Modulation for Capacitor Voltage Balancing of Three-Phase Three-Level Improved Power Quality Converter. *IET Power Electron.* **2014**, *7*, 973–983. [CrossRef]
30. Mondal, S.K.; Pinto, J.O.; Bose, B.K. A Neural-Network-Based Space-Vector PWM Controller for a Three-Level Voltage-Fed Inverter Induction Motor Drive. *IEEE Trans. Ind. Appl.* **2002**, *38*, 660–669. [CrossRef]
31. Tan, B.; Gu, Z.; Shen, K.; Ding, X. Third Harmonic Injection SPWM Method Based on Alternating Carrier Polarity to Suppress the Common Mode Voltage. *IEEE Access* **2018**, *7*, 9805–9816. [CrossRef]
32. Lei, W.; Shuanghui, H.; Minghui, H.; Baoyu, S. A Harmonic Injection SPWM Method for the High-Responsive PMSM Control System. *Int. J. Electron.* **2016**, *103*, 130–146. [CrossRef]
33. Wei, C.; Yuan, X.; Zhang, Y.; Wu, X. A Generic Multi-Level SVM Scheme Based on Two-Level SVM for N-Level Converters. *Energies* **2020**, *13*, 2143. [CrossRef]
34. Mini, Y.; Nguyen, N.K.; Semail, E.; Vu, D.T. Enhancement of Sensorless Control for Non-Sinusoidal Multiphase Drives-Part I: Operation in Medium and High-Speed Range. *Energies* **2022**, *15*, 607. [CrossRef]
35. Tian, Y.; Wickramasinghe, H.R.; Li, Z.; Pou, J.; Konstantinou, G. Review, Classification and Loss Comparison of Modular Multilevel Converter Submodules for HVDC Applications. *Energies* **2022**, *15*, 1985. [CrossRef]